

Enhancement of magnetic and dielectric properties of low temperature sintered NiCuZn ferrite by Bi_2O_3-CuO additives

Jie Li(李颉), Bing Lu(卢冰), Ying Zhang(张颖), Jian Wu(武剑), Yan Yang(杨燕), Xue-Ning Han(韩雪宁), Dan-Dan Wen(文丹丹), Zheng Liang(梁峥), and Huai-Wu Zhang(张怀武)

Citation: Chin. Phys. B, 2022, 31 (**4**): 047502. DOI: 10.1088/1674-1056/ac3399
Journal homepage: http://cpb.iphy.ac.cn; http://iopscience.iop.org/cpb

What follows is a list of articles you may be interested in

A review on 3d transition metal dilute magnetic *RE*In_3 intermetallic compounds

Xin-Peng Guo(郭新鹏), Yong-Quan Guo(郭永权), Lin-Han Yin(殷林瀚), and Qiang He(何强)
Chin. Phys. B, 2022, 31 (**3**): 037501. DOI: 10.1088/1674-1056/ac20cd

Tailoring the optical and magnetic properties of La-BaM hexaferrites by Ni substitution

Hafiz T. Ali, M. Ramzan, M Imran Arshad, Nicola A. Morley, M. Hassan Abbas, Mohammad Yusuf, Atta Ur Rehman, Khalid Mahmood, Adnan Ali, Nasir Amin, and M. Ajaz-un-Nabi
Chin. Phys. B, 2022, 31 (**2**): 027502. DOI: 10.1088/1674-1056/ac1412

Strain drived band aligment transition of the ferromagnetic VS_2/C_3N van der Waals heterostructure

Jimin Shang(商继敏), Shuai Qiao(乔帅), Jingzhi Fang(房景治), Hongyu Wen(文宏玉), and Zhongming Wei(魏钟鸣)
Chin. Phys. B, 2021, 30 (**9**): 097507. DOI: 10.1088/1674-1056/ac0cd1

Structure, morphology, and magnetic properties of high-performance NiCuZn ferrite

He Xue-Min, Yan Shi-Ming, Li Zhi-Wen, Zhang Xing, Song Xue-Yin, Qiao Wen, Zhong Wei, Du You-Wei
Chin. Phys. B, 2015, 24 (**12**): 127502. DOI: 10.1088/1674-1056/24/12/127502

Development and application of ferrite materials for low temperature co-fired ceramic technology

Zhang Huai-Wu, Li Jie, Su Hua, Zhou Ting-Chuan, Long Yang, Zheng Zong-Liang
Chin. Phys. B, 2013, 22 (**11**): 117504. DOI: 10.1088/1674-1056/22/11/117504

Enhancement of magnetic and dielectric properties of low temperature sintered NiCuZn ferrite by Bi_2O_3–CuO additives

Jie Li(李颉)[1,†], Bing Lu(卢冰)[1], Ying Zhang(张颖)[1], Jian Wu(武剑)[1], Yan Yang(杨燕)[1,2], Xue-Ning Han(韩雪宁)[1], Dan-Dan Wen(文丹丹)[3], Zheng Liang(梁峥)[1], and Huai-Wu Zhang(张怀武)[1]

[1] *State Key Laboratory of Electronic Thin Film and Integrated Devices, University of Electronic Science and Technology of China, Chengdu* 610054, *China*
[2] *College of Communication Engineering, Chengdu University of Information Technology, Chengdu* 610225, *China*
[3] *Chongqing Engineering Research Center of Intelligent Sensing Technology and Microsystem, Chongqing University of Post and Telecommunications, Chongqing* 400065, *China*

(Received 18 September 2021; revised manuscript received 20 October 2021; accepted manuscript online 27 October 2021)

With a series of 1.0 wt%Bi_2O_3–x wt% CuO (x = 0.0, 0.2, 0.4, 0.6, and 0.8) serving as sintering additives, $Ni_{0.23}Cu_{0.32}Zn_{0.45}Fe_2O_4$ ferrites are successfully synthesized at a low temperature (900 °C) by using the solid state reaction method. The effects of the additives on the phase formation, magnetic and dielectric properties as well as the structural and gyromagnetic properties are investigated. The x-ray diffraction (XRD) results indicate that the added Bi_2O_3–CuO can lower the synthesis temperature significantly without the appearing of the second phase. The scanning electron microscope (SEM) images confirm that Bi_2O_3 is an important factor that determines the sintering behaviors, while CuO affects the grain size and densification. With CuO content $x = 0.4$ or 0.6, the sample shows high saturation magnetization, low coercivity, high real part of magnetic permeability, dielectric permittivity, and small ferromagnetic resonance linewidth (ΔH). The NiCuZn ferrites are a promising new generation of high-performance microwave devices, such as phase shifters and isolators.

Keywords: NiCuZn ferrite, Bi_2O_3–CuO additive, magnetic properties, dielectric properties, ferromagnetic resonance (FMR) linewidth

PACS: 75.50.Gg, 75.47.Lx, 75.60.Ej, 75.75.Lf **DOI:** 10.1088/1674-1056/ac3399

1. Introduction

With the rapid development of the fifth generation of communication technology (5G), electronic devices continue their trend toward miniaturization, integration, multifunctionality, and in particular higher electromagnetic, frequencies. High frequency devices challenge researchers to the radio frequency (RF) applications.[1] Hence, a traditionally used magnetic material, NiCuZn ferrite, with high permeability, good chemical stability, low eddy-current loss, and high resistivity, benefit from enhanced properties to meet the modern requirements for high frequency device applications.[2–4] Considerable efforts have been already made to further improve the sintering properties, electrical resistivity, chemical stability, and permeability at intermediate to high frequencies.[5] To tune material properties, both the microstructure and magnetic properties of NiCuZn ferrites can be changed by adding different types of dopants. Many dopants, such as Bi_2O_3, CuO, V_2O_5, Co_2O_3, and combinations (B_2O_3–MoO_2, Bi_2O_3–Nb_2O_5), were introduced into NiCuZn ferrites to enhance their sintering and magnetic properties, but there has been no researches on dielectric properties of ferrites.[6–12]

The Bi_2O_3 and CuO were studied and found to be efficiently conducive to lowering the sintering temperature of ferrite. The Bi_2O_3 is an excellent liquid-phase sintering aid that can lower temperature and promote grain growth.[13–15] The CuO is also considered as a good sintering aid for NiCuZn ferrite.[16] Hence, the eutectic mixture of Bi_2O_3–CuO has a relatively low melting point below 800 °C, so that the doping of CuO and Bi_2O_3 is likely to facilitate the integrality of reaction and improve the densification of ferrite due to liquid-phase sintering. Xie *et al*. has used Bi_2O_3–CuO to lower the sintering temperature of LiZnTi ferrite and obtained a good microstructure and also good ferromagnetic properties, but there was no research on dielectric properties.[17] Therefore, the effect of Bi_2O_3–CuO additive on the microstructure, and properties of low-temperature-sintered NiCuZn ferrites, especially the dielectric and gyromagnet properties, were studied. The outcome of this study can be used for developing the low-temperature co-fired ceramics (LTCC) and producing electronic devices.

2. Experiment

The polycrystalline NiCuZn ferrite material ($Ni_{0.22}Cu_{0.20}Zn_{0.58}Fe_2O_4$), which contains different quantities of Bi_2O_3–CuO, were synthesized by using a solid state method. Firstly, raw materials, including NiO, CuO, ZnO, and Fe_2O_3, were weighed according to their stoichiometric ratio. Next, these powders were mixed in a ball and milled for 16 h. The obtained slurry was dried and pre-sintered at 800 °C for 4 h. Subsequently, the pre-sintered powders were doped

†Corresponding author. E-mail: lijie@uestc.edu.cn

© 2022 Chinese Physical Society and IOP Publishing Ltd

with 1 wt%Bi_2O_3–x-wt%CuO ($x = 0.0$ to 0.8 in steps of 0.2) and milled again for 12 h. The dried powders were pressed into toroidal samples with polyvinyl alcohol (PVA) under a pressure of about 10 MPa. Finally, the samples with different Bi_2O_3–CuO additives were sintered at 900 °C for 4 h.

The phase formation of the samples was characterized by using x-ray diffraction (XRD, Cu $K\alpha$ radiation, Rigaku, Japan). The microstructures were examined with a scanning electron microscope (SEM, JSM-6490, JEOL). The bulk density of the sample was evaluated by using the Archimedes method in distilled water. The complex permeability was measured by using an impedance analyzer (E4991B, Agilent). Vibrating sample magnetometer (VSM, MODEL, BHL-525, Japan) measurements, with ±2500 Oe (1 Oe = 79.5775 A·m^{-1}) magnetic field, were carried out to investigate the magnetic properties. The ferromagnetic resonance (FMR) linewidth (ΔH) of the samples required the preparation of the spherical samples with a diameter of about 1.0 mm. They were measured by using the TE106 cavity perturbation method at 9.55 GHz.

3. Results and discussion

The XRD patterns for samples with different Bi_2O_3–CuO content are shown in Fig. 1. The crystal planes are indexed, according to their diffraction peaks, to (220), (311), (222), (400), (422), (511), and (440) (see Fig. 1). The results indicate that a pure spinel phase of NiCuZn ferrite is obtained after sintering at 900 °C. Furthermore, the Bi_2O_3–CuO additive is able to lower the sintering temperature of sample and facilitate the synthesis of NiCuZn ferrite. In addition, it can be seen that there is no shift toward higher nor lower angles with increasing the amount of Bi_2O_3–CuO additive, indicating that the Bi^{3+} ion does not enter into the lattice site nor change the lattice shape. Furthermore, neither a CuO phase nor any other related second phase appears in the XRD results, showing that the increased CuO phase has entered into the crystal lattice, occupying the lattice vacancies, and enhancing the properties of the sample.

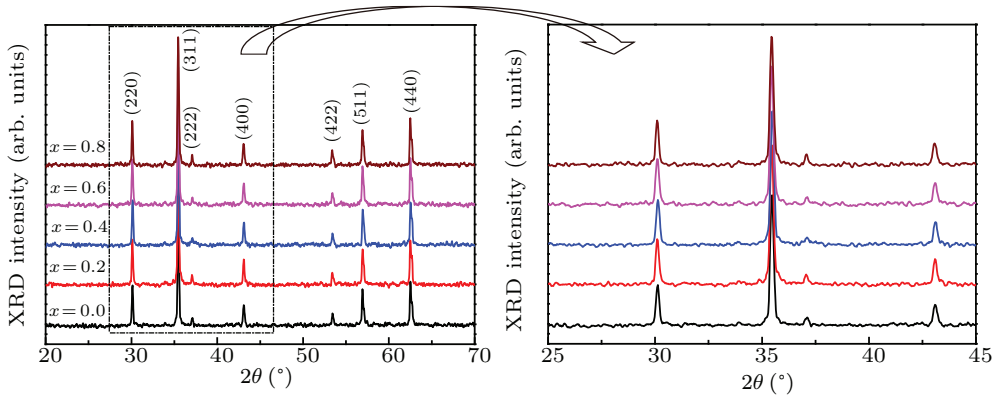


Fig. 1. XRD patterns of samples with different Bi_2O_3–CuO additives.

Both the microstructure and morphology of ferrites can provide valuable information to understand the sintering properties and the effects on the physical and chemical properties of ferrite. The cross-section SEM images and the bulk density of the samples are shown in Fig. 2. All samples are densely sintered, while the Bi_2O_3 additive accelerates the synthesis of NiCuZn ferrites and promotes the grain growth. Moreover, the grain sizes in these samples are slightly different from each other. For all samples, because the constant x of the Bi_2O_3 additive is kept unchanged, while the constant x of the CuO additive is varied, the observed difference in grain-size difference ought to originate from the CuO effect. In NiCuZn ferrite, there are 32 octahedral sites (B-sites), and Cu^{2+} ion preferred to occupy octahedral site (B site).[18] All the metal ions occupy 16 B-sites, so there are 16 vacancy locations at B-sites. Hence, in the present study, the content of CuO is slight, and the CuO preferred to occupy the lattice vacancies (B-sites). Hence the grain size of sample is little changed. In addition, the constant x of the CuO additive is small, and it does not generate a second phase. Hence, the SEM images reveal the characteristic shape of spinel NiCuZn ferrites, which is the main cause for the magnetic and dielectric properties of the samples.

Figure 2 also shows the bulk density of the sample. The bulk density is calculated from the following formula:

$$\rho = \frac{W_1}{W_1 - W_2} \times \rho_{H_2O},$$

where W_1 is the weight of the sample in air, and W_2 is the weight of the sample in distilled water. The bulk density of the NiCuZn ferrite is improved significantly by using the Bi_2O_3–CuO additive. The maximum value of the bulk density is 5.04 g/cm^3. The bulk density first increases and then decreases. Based on the value of saturation magnetization and coercivity (as shown in Fig. 5), the reason for this may be that the Cu^{2+} ions first occupy the lattice vacancies (before $x = 0.4$) and they are located at the grain boundaries (after $x = 0.4$).[19]

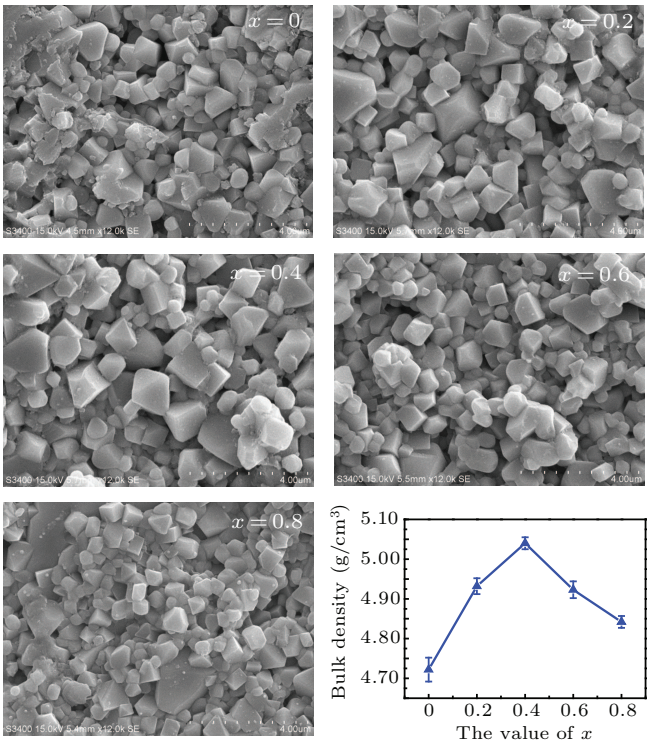


Fig. 2. SEM images and bulk density of samples with different Bi_2O_3–CuO additives.

The XPS measurements are carried out to further analyze the cation oxidation states and the chemical composition of synthesized samples, for they closely relate to the catalytic activity of metal oxides. The Fe 2p x-ray photoelectron spectroscopy (XPS) spectra for all the samples are displayed in Fig. 3. Both the detailed binding energy (BE) obtained from the Gaussian fitting and the assignments for each peak are accomplished by comparing with the data from the literature.[20] The Fe 2p spectra are composed of two spin-orbit doublets characteristics of Fe $2p_{3/2}$ (710.5 eV, Fe^{3+} in octahedral site, and 712.5 eV, Fe^{3+} in tetrahedral site) and Fe $2p_{1/2}$ (724.2 eV, Fe^{3+} in octahedral site, and 726.8 eV, Fe^{3+} in tetrahedral site) and two shakeup satellites at 718.1 eV, 732.8 eV, respectively. The area ratios of Fe^{2+}:Fe^{3+} are 2.84:2.6, 3.61:2.58, 4.1:2.51, 4.51:2.6, and 4.39:2.51, ascending with the Bi_2O_3–CuO additive content increasing. The proportion of Fe^{2+} ion was increasing with Bi_2O_3–CuO additive increasing, which attests that part of O^{2-} ions provide electrons and form chemical bonds with Cu^{2+} ion. In the present research, in $Ni_{0.22}Cu_{0.20}Zn_{0.58}Fe_2O_4$ ferrite, Ni, Cu, Zn, and Fe ions occupy corresponding crystalline sites. Hence, the Cu^{2+} ion additive prefers to occupy the lattice vacancy. The changes of Fe^{2+} ions and Fe^{3+} ions also attest to this fact.

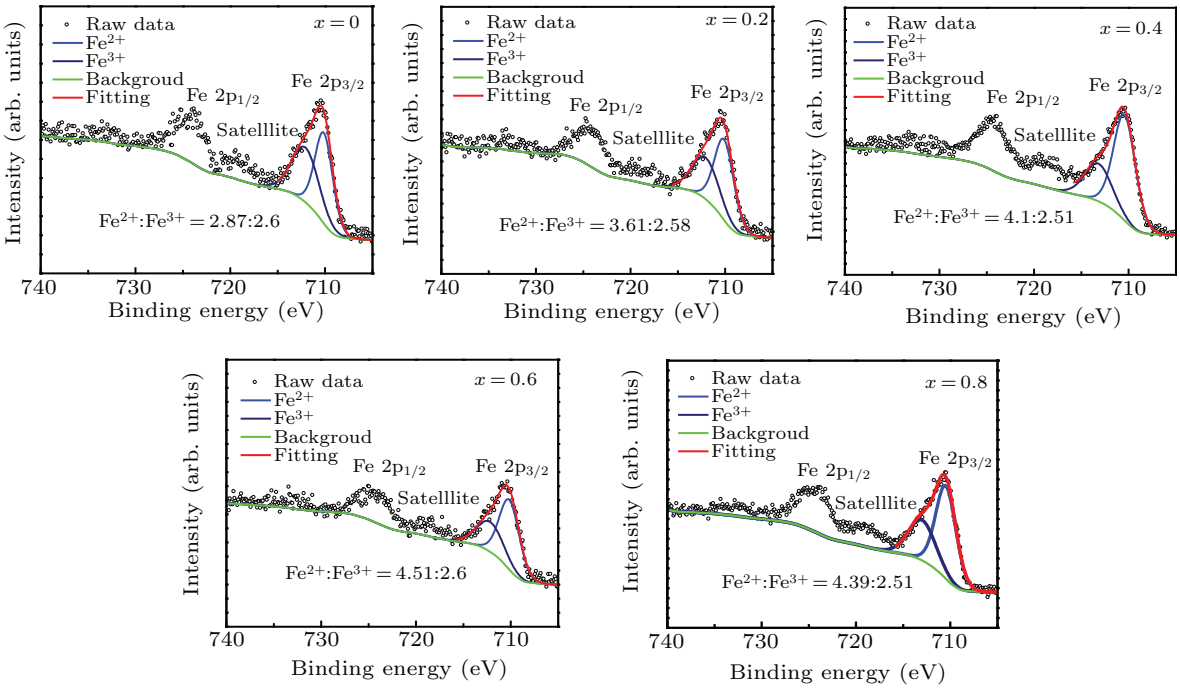


Fig. 3. Fe 2p XPS spectra of samples with different Bi_2O_3–CuO additives.

The magnetic hysteresis loops for the different samples are illustrated in Fig. 4. These curves reveal a characteristic soft magnetism. Variations in the saturation magnetization (M_s) and coercivity (H_c) of the samples are shown in Fig. 5. With the increasing of Bi_2O_3–CuO additive constant, the saturation magnetization of the sample first increases to a maximum value ($x = 0.4$, $M_s = 27.97$ emu/g) and then decreases. In addition, the coercivity first decreases to a minimum value ($x = 0.2$, $H_c = 28.65$ Oe) and then increases. The proportion of Fe^{2+} ion decreases with Bi_2O_3–CuO additive increasing, which is shown in Fig. 3. Most of Cu^{2+} ions occupy the octahedral sites, and the Fe^{2+} ions prefer to occupy the tetrahedral sites. The coercivity of sample ($x = 0.2$) ferrite is smaller than those of other samples, which was also reported by Yang and

Luo.[21]

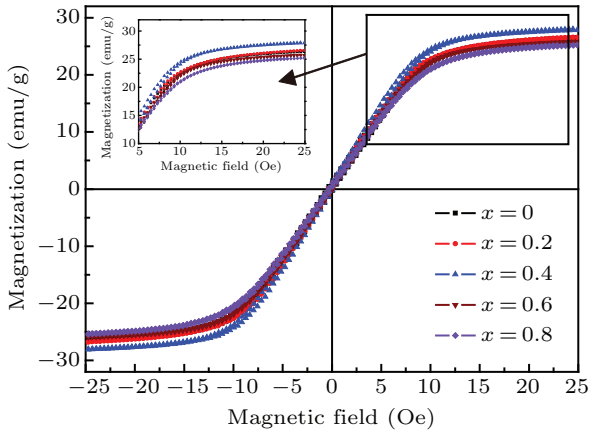


Fig. 4. Magnetic hysteresis loops of samples with different Bi_2O_3–CuO additives.

For the ferrite, the magnetic properties are affected by the chemical composition and ion distribution at the crystallographic site. In this study, both the saturation magnetization and the coercivity are determined by using the chemical formula for $Ni_{0.22}Cu_{0.20}Zn_{0.58}Fe_2O_4$. The changes are affected by both the Bi_2O_3 additive and the CuO additive. First, 1-wt% Bi_2O_3 additive can lower the sintering temperature and promote the synthesis of NiCuZn ferrites,[8] while the CuO additive changes the magnetic properties. For $x = 0.0$, the pure NiCuZn ferrite has a saturation magnetization of 26.45 emu/g. With CuO increasing, the Cu^{2+} ion can occupy the lattice vacancies (octahedral sites), leading to enhanced magnetic properties. For $x = 0.6$ and 0.8, some of the Cu^{2+} ions exist at the grain boundaries and form Cu–O bonds. This has a deteriorating effect on magnetic properties of the samples. Second, the variation of M_s might be due to the larger grains of ferrites. The SEM images show that the samples with $x = 0.4$ and 0.6 have both a larger grains size. Finally, the bulk density is another factor to change the magnetic properties. The sample with $x = 0.4$ shows high densification, which leads to higher saturation magnetization.

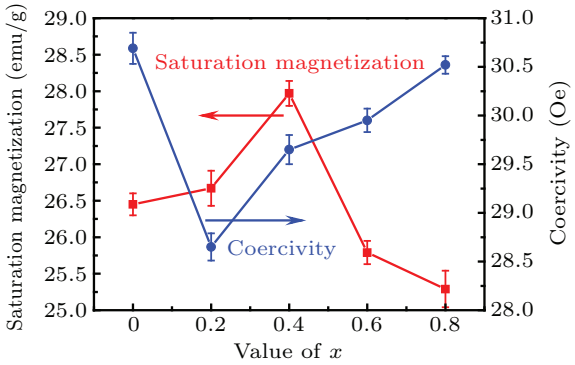


Fig. 5. Variations of saturation magnetization (M_s) and coercivity (H_c) with the values of x for samples with different Bi_2O_3–CuO additives.

The values of coercivity (H_c) of the samples show the opposite trend to the variation in M_s, and the changes of H_c are mainly due to chemical composition and CuO additive. The Cu^{2+} ions occupied positions are the main factor changing the value of H_c. The Cu^{2+} ions in lattice vacancy and grain boundary, especially in the grain boundary, Cu^{2+} ions impede the motion of domain wall, which results in the increase of H_c when x is larger than 0.4. the formation of CuO precipitates during the sintering of NiCuZn ferrites can be attributed to the sintering process being faster than oxygen diffusion from outside into the pores. This phenomenon has been reported by Barba *et al.*[22] and Hsiang and Chuch.[22,23] Moreover, H_c is also determined by the density and microstructure of the ferrite sample. The high densification and high average grain size lead to a low H_c. Furthermore, when an extra amount of Bi_2O_3–CuO is present at the grain boundary, which can promote a chemical reaction, the demagnetizing field increases at the grain boundaries, which also contributes to the increase of H_c.

Figure 6 shows the curves of frequency-dependent complex magnetic permeability of samples with different amounts of Bi_2O_3–CuO additive. The real part of magnetic permeability (μ') first increases up to a maximum value and then decreases. For $x = 0.0$, the value of μ' is about 184.8 at 1 MHz–5 MHz, and the maximum value of μ' is about 210.2 at 1 MHz–5 MHz for $x = 0.6$. In addition, the imaginary part of the magnetic permeability (μ'') remains small, which attests that the material has low magnetic loss. The NiCuZn ferrite possesses a good complex magnetic permeability and can be used in electronic devices. In this study, the Bi_2O_3 lowers the sintering temperature significantly, leading to high densification. The CuO additive is an important factor as far as the change of the complex magnetic permeability is concerned. As discussed above, some CuO particules can enter into the lattice vacancies, thereby improving the magnetic properties, and superfluous CuO is present along the grain boundary, which creates a negative effect on the magnetic properties. However, the maximum value of μ' occurs for $x = 0.6$, which is different from the saturation magnetization. For the NiCuZn ferrite, μ' is correlated with the spin rotation and the domain wall motion. The domain wall motion represents a dominant contribution to the magnetization mechanism and can be described as follows:[7,24]

$$\mu' = 1 + \mu_w + \mu_{spin} = \frac{2\pi M_s^2 D}{4\gamma} + \frac{2\pi M_s^2}{K}.$$

Here, μ_w is the domain wall susceptibility, μ_{spin} the intrinsic rotational susceptibility, M_s the saturation magnetization, D the grain size, γ the domain wall energy, and K the magneto-crystalline anisotropy constant. Hence, the addition of CuO can affect the grain size and magneto-crystalline anisotropy, which causes the μ' value of $x = 0.6$ sample to be higher than that of $x = 0.4$ sample.

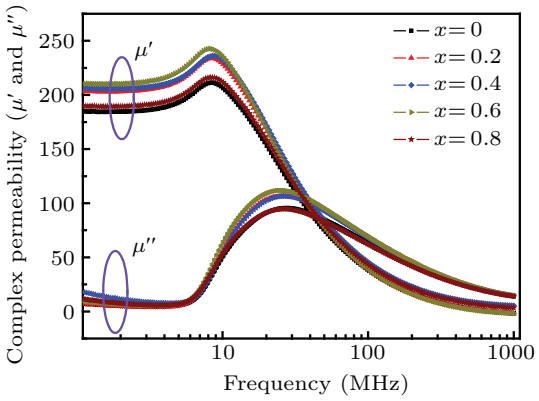


Fig. 6. Complex magnetic permeability (μ' and μ'') of samples with different Bi_2O_3–CuO additives.

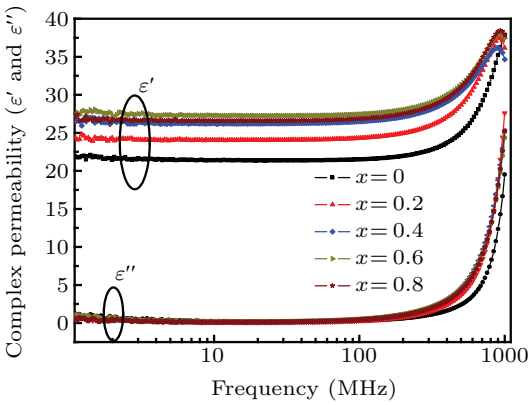


Fig. 7. Curves of frequency-dependent complex dielectric permittivity (ε' and ε'') of samples with different Bi_2O_3–CuO additives.

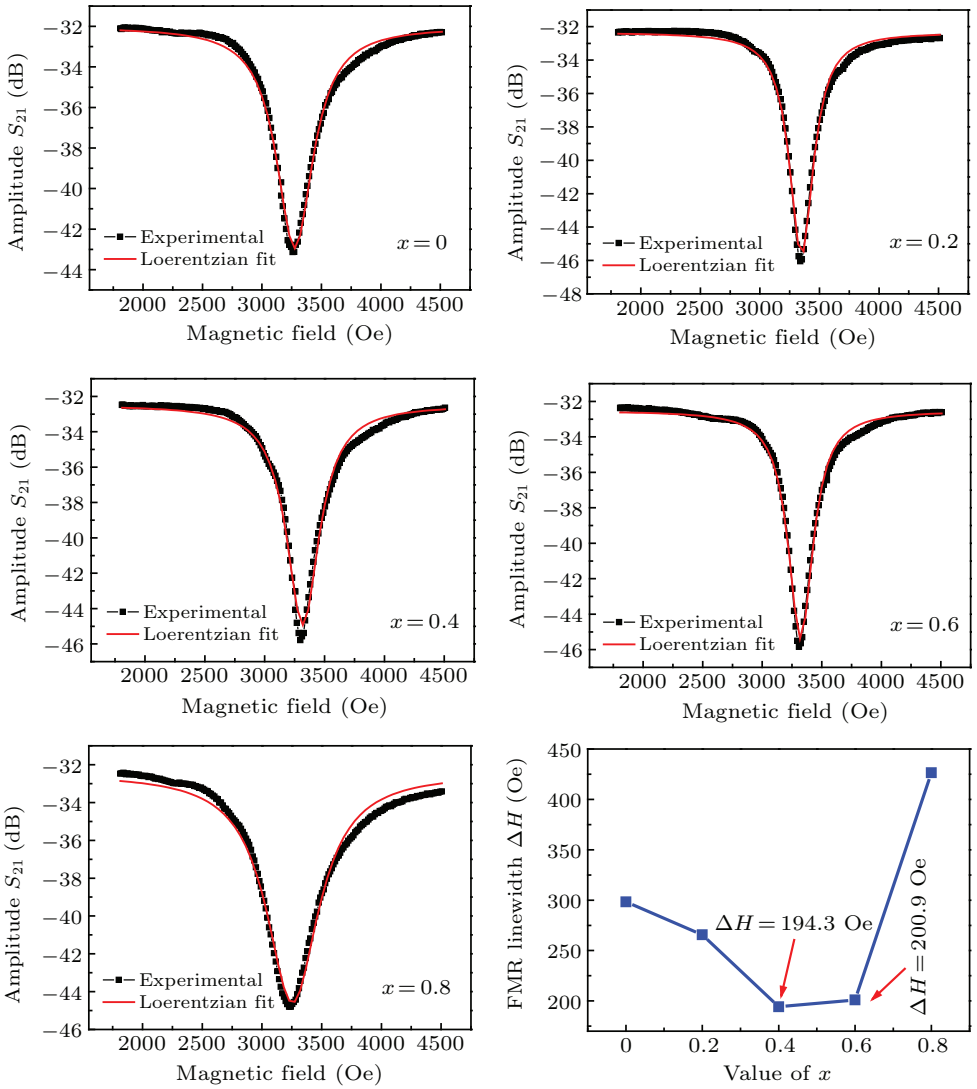


Fig. 8. Ferromagnetic resonance (FMR) linewidths based on fitting of Lorentzian to spectra of the samples.

Figure 7 shows the curves of frequency-dependent complex dielectric permittivity (ε' and ε'') of samples with different Bi_2O_3–CuO additives. The dielectric permittivity curves show a similar trend with magnetic permeability increasing. The maximum value of the real part of the permittivity (ε') is about 27.23 for $x = 0.6$. Each of these samples possesses a low imaginary part for the permittivity. The dielectric properties for each of ferrites show a strong relation with hopping of electrons at the octahedral site. The electron exchange between Fe^{2+} and Fe^{3+}, results in a local displacement of the electrons, thereby inducing the polarization.[3] The Cu^{2+} ions occupy the lattice vacancies of the ferrite, forming covalent

bonds with O^{2-} ions, which causes the number of Fe^{2+} ions in the ferrite to increase. Furthermore, the electron hopping probability of Fe^{3+}–Fe^{2+} increases with the number of Cu^{2+} ions increasing, thus leading the ε' to augment. However, with the further increase of Cu^{2+} ions, the superfluous CuO exerts a negative effect on the dielectric properties. According to the Debye relaxation model, the electric field changes more slowly than the relaxation of materials and the polarization can change with electric field very well at the low frequency, which results in the imaginary part of complex permittivity (ε'') tending to the real part of complex permittivity (ε'). In addition, figure 7 shows that there exists a turning corner for each of these samples while the test frequency is nearly 1 GHz. In ferrite ceramics, the grain boundaries represent a barrier which weakens the electrons hopping, causing the inter-grain conductivity to drop. In addition, owing to the high resistance of grain boundaries, electrons accumulate at grain boundaries and produce space charge polarization. At high frequencies, the constancy of both ε' and ε'' can be attributed to the fact that the electrons in the grain can no longer follow the alternating field. This is in good agreement with previous results.[25,26]

Figure 8 shows the ferromagnetic resonance (FMR) linewidth (ΔH) of Lorentz fitting to NiCuZn ferrites with different Bi_2O_3–CuO additives. The ΔH values for different CuO additives are shown in Fig. 8. The value of ΔH first decreases, reaching a minimum value and then increasing. The smallest ΔH value is about 194.3 Oe for $x = 0.4$. Evidently, the different chemical compositions can have a dramatic effect on ΔH value. Also, the grain size distribution, pores, and microstructure play a key role in lowering the ΔH value.[27] In this study, the difference in ΔH value can be attributed to the correlation between the grain size distribution and Cu^{2+} ion occupancy. Firstly, based on the SEM images (Fig. 2), the samples with $x = 0.4$ and 0.6 have bigger grain sizes, which can enhance the gyromagnetic properties considerably (lower ΔH). Secondly, the densification affects the value of ΔH. The higher the densification of the ferrite, the lower the magnetic loss is. Hence, the samples with higher density show lower ΔH value. Finally, the $x = 0.8$ sample has a higher value for ΔH ($\Delta H = 426.4$ Oe). This can be explained by the fact that Cu^{2+} ions exist along the grain boundary that hinder the domain walls from displacing. Of course, based on the discussion above, the change of ΔH can also be expressed as

$$\begin{aligned}\Delta H &= \Delta H_{\text{int}} + \Delta H_{\text{a}} + \Delta H_{\text{p}} \\ &= \Delta H_{\text{int}} + 2.07\frac{H_{\text{a}}^2}{4\pi M_{\text{s}}} + 1.5\,(4\pi M_{\text{s}})\,P.\end{aligned}$$

Here, ΔH_{int} is the intrinsic linewidth, H_{a} the random anisotropy field, and P attributed to the porosity of grains. In this study, the effect of grain size, densification, and ion occupancy are discussed and the material is found to have potential applications in microwave devices.

4. Conclusions

In summary, the NiCuZn ferrite are successfully synthesized with Bi_2O_3–CuO as additives in a low-temperature sintering process. The addition of Bi_2O_3–CuO can enhance the microstructure and magnetic properties. The CuO particles can either occupy lattice vacancies or be located along the grain boundaries, which affects the microstructure and properties considerably. The samples show excellent magnetic and dielectric properties, when $x = 0.4$ and $x = 0.6$. Hence, it is expected that the NiCuZn ferrites with optimal additives could be a promising material for microwave devices.

Acknowledgements

Project supported by the National Key Research and Development Program of China (Grant No. 2018YFE0115500), the National Natural Science Foundation of China (Grant Nos. 52003256 and 51902037), and the Natural Science Foundation of Shanxi Province, China (Grant No. 201901D211259).

References

[1] Yang Y, Li J, Zhang H W, Wang G, Gan G W and Rao Y H 2020 *J. Mater. Sci.-Mater. El.* **31** 12325
[2] Frajer G, Isnard O, Chazal H and Delette G 2019 *J. Magn. Magn. Mater.* **473** 92
[3] Yan S Q, Liu S, He J, Luo H, He L H, Li Y H, Huang S X and Deng L W 2018 *J. Magn. Magn. Mater.* **452** 349
[4] Wang A P, Su H, Tang X L, Li Y X, Xu Z Q and Jing Y L 2018 *J. Mater. Sci.-Mater. El.* **29** 14605
[5] Wang Y, Jing Y L, Wang P, Li Y X, Lu Q H and Tang X L 2020 *J. Magn. Magn. Mater.* **514** 167182
[6] Wang X Y, Zhang D N, Wang G, Jin L C, Li J, Liao Y L, Zhang H W and Wang S Y 2020 *Ceram. Intl.* **46** 10652
[7] Yang Y, Zhang H W, Li J, Xu F, Gan G W and Wen D D 2018 *Ceram. Intl.* **44** 10545
[8] Luo Q, Su H, Tang X L, Xu Z Q, Li Y X and Jing Y L 2018 *Ceram. Intl.* **44** 16005
[9] Zhu H, Shen W, Zhu H, Jin Y and Zhou H 2014 *Ceram. Intl.* **40** 10985
[10] Kabbur M, Waghmare S D, Ghodake U R and Suryavanshi S S 2018 *AIP Conference Proceedings* **1942** 130002
[11] Hsiang H I, Yang S M and Chen C C 2020 *Int. J. Appl. Glass Sci.* **11** 774
[12] Han J M, Sun L, Cao E S, Hao W T, Zhang Y J and Ju L 2021 *Chin. Phys. B* **30** 096102
[13] Meng F B, Yang M, Zhao L, Zhang Y J, Shang X N, Jin P and Zhang W 2017 *Ceram. Intl.* **43** 15959
[14] Zhang S N, Jia L J, Zhang H W, Li J, Zhou T C and Liu B Y 2014 *J. Appl. Phys.* **115** 17A524
[15] Zheng Y H, Jia L J, Xu F, Wang G, Shi X L and Zhang H W 2019 *Ceram. Intl.* **45** 22163
[16] Mondal R A, Murty B S and Murthy V R K 2014 *J. Alloys Compd.* **595** 206
[17] Xie F, Jia L J, Zhao Y P, Li J, Zhou T C, Liao Y L and Zhang H W 2017 *J. Alloys Compd.* **695** 3233

[18] Yang W, Kan X C, Liu X S, Wang Z Z, Chen Z H, Wang Z, Zhu R W and Shezad M 2019 *Ceram. Intl.* **45** 23328
[19] Ribeiro U L, Nasar R S, Nasar M C and de Araujo J H 2018 *Ceram. Intl.* **44** 723
[20] Zhao X, Fu Y, Wang J, Xu Y J, Tian J H and Yang R Z 2016 *Electrochimica Acta* **201** 172
[21] Yan Z and Luo J H 2017 *J. Alloys Compd.* **695** 1185
[22] Barba A, Clausell C, Nuno L and Jarque J C 2017 *J. Eur. Ceram. Soc.* **37** 169
[23] Hsiang H I and Chueh J F 2015 *Intl. J. Appl. Ceram. Technol.* **12** 1008
[24] Xie F, Liu H, Zhou S, Chen Y, Xu F, Bai M Y and Liu W G 2021 *J. Alloys Compd.* **862** 158650
[25] Hcini F, Hcini S, Wederni M A, Alzahrani B, Al Robei H, Khirouni K, Zemni S and Bouazizi M L 2022 *Physica B* **624** 413439
[26] Hcini S, Omri A, Boudard M, Bouazizi M L, Dhahri A and Touileb K 2018 *J. Mater. Sci.-Mater. El.* **29** 6879
[27] Yang Y, Li J, Zhang H W, Rao Y H, Wang G and Gan G W 2020 *J. Mater. Sci.-Mater. El.* **31** 2845